ILASS–Europe 2017, 28th Conference on Liquid Atomization and Spray Systems, 6-8 September 2017, Valencia, Spain
http://dx.doi.org/10.4995/ILASS2017.2017.5040

CFD simulations of the diesel jet primary atomization from a multihole injector

C. A. Chasos*[1]
[1]Mechanical Engineering Department, Frederick University, Nicosia, Cyprus
*Corresponding author: eng.cca@fit.ac.cy

Abstract
High pressure multi-hole diesel injectors are currently used in direct-injection common-rail diesel engines for the improvement of fuel injection and air/fuel mixing, and the overall engine performance. The resulting spray injection characteristics are dictated by the injector geometry and the injection conditions, as well as the ambient conditions into which the liquid is injected. The main objective of the present study was to design a high pressure multi-hole diesel injector and model the two-phase flow using the volume of fluid (VOF) method, in order to predict the initial liquid jet characteristics for various injection conditions. A computer aided design (CAD) software was employed for the design of the three-dimensional geometry of the assembly of the injector and the constant volume chamber into which the liquid jet emerges. A typical six-hole diesel injector geometry was modelled and the holes were symmetrically located around the periphery of the injector tip. The injector nozzle diameter and length were 0.2 mm and 1 mm, respectively, resulting in a ratio of nozzle orifice length over nozzle diameter L/D = 5. The commercial computational fluid dynamics (CFD) code STAR-CD was used for the generation of the computational mesh and for transient simulations with an Eulerian approach incorporating the VOF model for the two-phase flow and the Rayleigh model for the cavitation phenomenon. Three test cases for increasing injection pressure of diesel injection from the high pressure multi-hole diesel injector into high pressure and high temperature chamber conditions were investigated. From the injector simulations of the test cases, the nozzle exit velocity components were determined, along with the emerging liquid jet breakup length at the nozzle exit. Furthermore, the spray angle was estimated by the average radial displacement of the liquid jet and air mixture at the vicinity of the nozzle exit. The breakup length of the liquid jet and the spray cone angle which were determined from the simulations, were compared with the breakup length and cone angle estimated by empirical equations. From the simulations, it was found that cavitation takes place at the nozzle inlet for all the cases, and affects the fuel and air interaction at the upper area of the spray jet. Furthermore, the spray jet breakup length increases with elapsed time, and when the injection pressure increases both the breakup length and the spray cone angle increase.

Keywords
Diesel injector, VOF, atomization.

Introduction

The main objective of the present work was to characterize the flow phenomena at the exit of the nozzle of a multi-hole Diesel injector. It was of main interest to examine the behaviour of the emerging two-phase flow spray jet with emphasis in the primary spray jet atomization. The objectives included, first the setup of the CFD model for a typical three-dimensional valve-covered orifice (VCO) sac-less six-hole diesel injector for carrying out the analysis of the initial spray characteristics, namely the liquid breakup length and the spray angle at the nozzle exit. The second objective was the calculation of the primary atomization characteristics with empirical equations and to compare the empirical data with the simulations. The injector which was used had sharp nozzle entry, a nozzle diameter equal to 0.2 mm and a ratio of nozzle orifice length over nozzle diameter L/D = 5.

Previous experimental [1, 10, 14, 15] and computational [1, 6, 9, 11, 13] studies investigated the internal and external flow of diesel injectors. In some experiments, large scale transparent injectors were used [8], [12], and it was found that cavitation phenomena are present. Experimental studies [10, 14] revealed that the emerging liquid jet is affected by both cavitation and the interaction with the surrounding gas flow. Various methodologies were adopted for injector flow simulations, including the VOF method [8] and the large eddy simulation (LES) framework [5]. The simulations from previous studies revealed that strong vortex structures were generated around the liquid jet penetrating in the gas phase and these were the results of velocity relaxation inside the liquid [8]. However, as it was reported in [8], the problem of jet disintegration is complex and not well understood.

The effect of injection pressure on the initial spray atomization characteristics predicted from simulations and comparisons with pertinent data estimated from empirical models, have not been found by the author of the

present work in published work. Thus, it is required to quantify the effects of the injection pressure on the injected spray jet, as well as compare the primary spray atomization characteristics from simulations with data from empirical equations. In the present work, the adopted CFD methodology is described first. Then, the results for three test cases at low, medium and high injection pressure of the diesel injector into high pressure and high temperature chamber conditions are presented. Finally, conclusions and recommendations are provided.

Methodology

The CFD methodology along with the simulations setup are described first, followed by the illustration of the empirical equations which were used for the calculation of the liquid jet breakup length and the spray jet angle.

For the CFD simulations, the CFD code STAR-CD [3] was used. The Eulerian modelling methodology employing the VOF method was utilized, which included the mass, momentum and energy conservation equations for the two phases. The interface-capturing method in the VOF method was employed, by computing the convective terms in the volume fraction equations using the High-Resolution Interface-Capturing (HRIC) model [3]. For the two-phase flow modelling, the pressure in the two phases was assumed to be the same. A constant value of surface tension was used, with which the normal force due to the surface tension is treated using the continuum surface force (CSF) model [3], while the tangential force is not accounted. The CSF model provides a source term in the momentum conservation equation. The turbulence was modelled with the k-ε high Reynolds number RNG model [17], and the boundary layer was handled with the standard wall functions. The MARS [3] differencing scheme was used for the discretization of the conservation equations. Transient simulations were carried out, and the SIMPLE algorithm [3] was employed for the numerical solution of the problem.

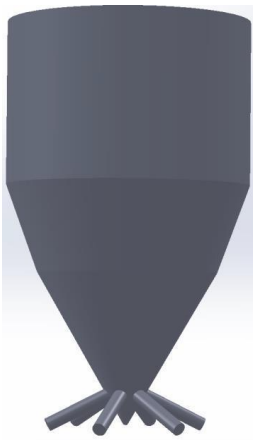

Figure 1. Three-dimensional injector geometry design.

A VCO sac-less six-hole diesel injector and a constant volume chamber were assembled for the computational mesh generation. The injector design was based on typical injector geometries found from literature ([10, 11, 14, 15]). The three-dimensional injector which was designed with a CAD software [4] is shown in Figure 1. The injector design was for a six-hole diesel injector whose nose holes were symmetrically located around the periphery of the injector tip as shown in Figure 1. The nozzle entry was designed with sharp edge at the body of the injector. The injector nozzle diameter and length were 0.2 mm and 1 mm, respectively, resulting in a ratio of nozzle orifice length over nozzle diameter L/D = 5. The designed constant volume chamber had length 5 mm which corresponds to 25 D distance downstream the nozzle, and a square cross-sectional area with side width 1 mm. The constant volume chamber was assembled at the tip of the nozzle exit, and the centreline of the nozzle and the symmetry axis of the chamber coincided. The computational mesh was generated with the automatic mesh generation tool of STAR-CD [3], where prism type cells computational were used. The resulting mesh was composed of around 850000 cells and it is presented in Figure 2. The cell size ranged from 5 to 10 μm within the injector and the cell size varied between 10 to 20 μm in the constant volume chamber. Figure 2 includes the boundary conditions which were imposed for the simulation setup. Inlet boundary condition was defined at the entry of the injector on the top, shown in dark yellow color in Figure 2. Symmetry plane boundary conditions were imposed on the symmetry sides of the one-sixth segment of the injector, which are presented in violet color in Figure 2. No-slip wall boundary condition was imposed on the four sides of the chamber, which is indicated with orange color in Figure 2. Wall boundary condition was set at the remaining surfaces, including the injector shell, the nozzle and the back plane of the chamber where the nozzle tip was assembled. Pressure boundary condition

was defined at the chamber front plane. At the pressure boundary, the pressure and temperature were set equal to 42 bar and 1000 K, respectively, which resemble diesel engine conditions during compression stroke.

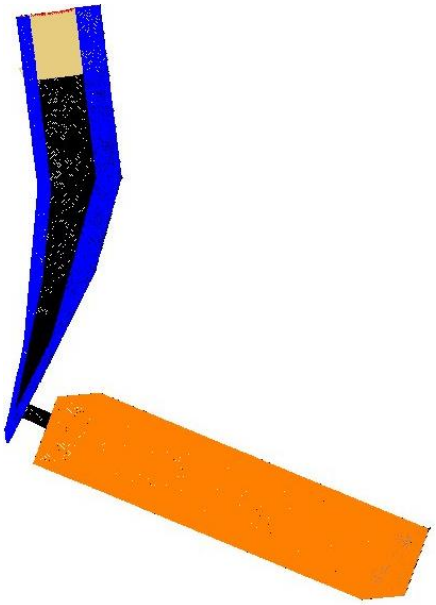

Figure 2. Computational mesh and boundary conditions.

At the inlet boundary, the volume fraction of the fuel was set equal to 1 and uniform inlet velocities for the three test cases were defined. The code uses the inlet velocity and calculates the injection pressure at the inlet. For the simulations, n-heptane and air were utilized. The properties of n-heptane liquid, n-heptane vapour and air from the database of STAR-CD [3] were employed, and are contained in Table 1.

Table 1. Physical properties of the fuel and air.

Property	Liquid n-heptane	Vapour n-heptane	Air
Density (Kg/m^3)	678.3	2.48639	1.18415
Molecular viscosity (Kg/ms)	3.92073 10^{-4}	1.01377 10^{-5}	1.855 10^{-5}
Surface tension coefficient (N/m)	0.0727		

For the initial conditions of the transient simulations, stagnant air was set in the computational domain. The simulations for the three test cases were performed for an injection duration of 1 ms. The computational time step size was constant and equal to 0.5 μs. The numerical processing of the simulations was performed on a sequential computer. The simulation results are presented and discussed in the next section.

In the present work, in the absence of experimental data for validation of the simulations, empirical equations were used in order to obtain data for comparison with the simulations. Empirical equations provide the primary atomization characteristics and are usually employed within the atomization modelling setup in diesel engine CFD simulations. From a literature survey, the empirical equations for the calculation of the breakup length and spray angle were adopted from [15] and [2], respectively. The liquid jet breakup length was estimated by the following empirical equation (from [15]),

$$L = 0.39\,(2\,\Delta p/\rho_l)^{1/2}\,t \tag{1}$$

where Δp is the pressure drop along the nozzle, ρ_l is the liquid density and t is the elapsed time after the start of injection. The cone angle for diesel jet spray in the atomisation region was calculated from the empirical equation of Arai [2] by,

$$\theta = 0.017\left(\frac{D^2\rho_a\,\Delta p}{\mu_a^2}\right)^{0.25} \tag{2}$$

where D is the nozzle diameter, ρ_a is the density of air in the chamber and μ_α is the molecular viscosity of air.

Results

In the present section, the results and discussion from the simulations for the three test cases are presented. For the test cases, the injection pressure was calculated by the code at the inlet boundary. The velocity at the inlet boundary, the resulting injection pressure and the mass flow rate of fuel are included in Table 2. The three cases denoted, low, medium and high injection pressure correspond to modern common rail system injection pressure. As it can be seen in Table 2, the injection pressure was 1124, 1669 and 2245 bar.

Table 1. Test cases conditions.

Test case	Description	Inlet velocity (m/s)	P_{inj} (bar)	*Fuel mass flow rate (Kg/s)*
1	Low injection pressure	20	1124	0.0422
2	Medium injection pressure	24	1669	0.0507
3	High injection pressure	28	2245	0.0592

First, the evolution of the VOF field from the simulations at the vertical symmetry section plane of the nozzle and the chamber are presented in Figure 3, 4 and 5. Then, comparisons of the VOF field and the velocity field between the three cases at 0.25 ms after start of injection (ASOI) are presented. Finally, the breakup length and spray ject cone angle from the simulations are compared with the empirical data.

For the low injection pressure, Case 1, the evolution of the liquid fuel injection and the propagation of the emerging fuel jet are presented with the VOF flow field in Figure 3. From the simulations of Case 1, it was found that the fuel starts to emerge from the nozzle exit at 0.2 ms after the start of the simulation. As it can be seen in Figure 3, there is cavitation area which is created at the upper edge of the nozzle inlet. The axial penetration of the spray jet increases with elapsed time, and at 0.3 ms the spray reaches the chamber front plane. Also, the spanwise spreading of the two-phase spray jet increases with time. A spray jet with VOF higher than 0.5, indicated with green colour, is present at the nozzle exit, which increases with time. For this case the spray jet slightly bends at an angle of around 10°, which is the effect of the induced gas recirculation at the upper area of the spray jet.

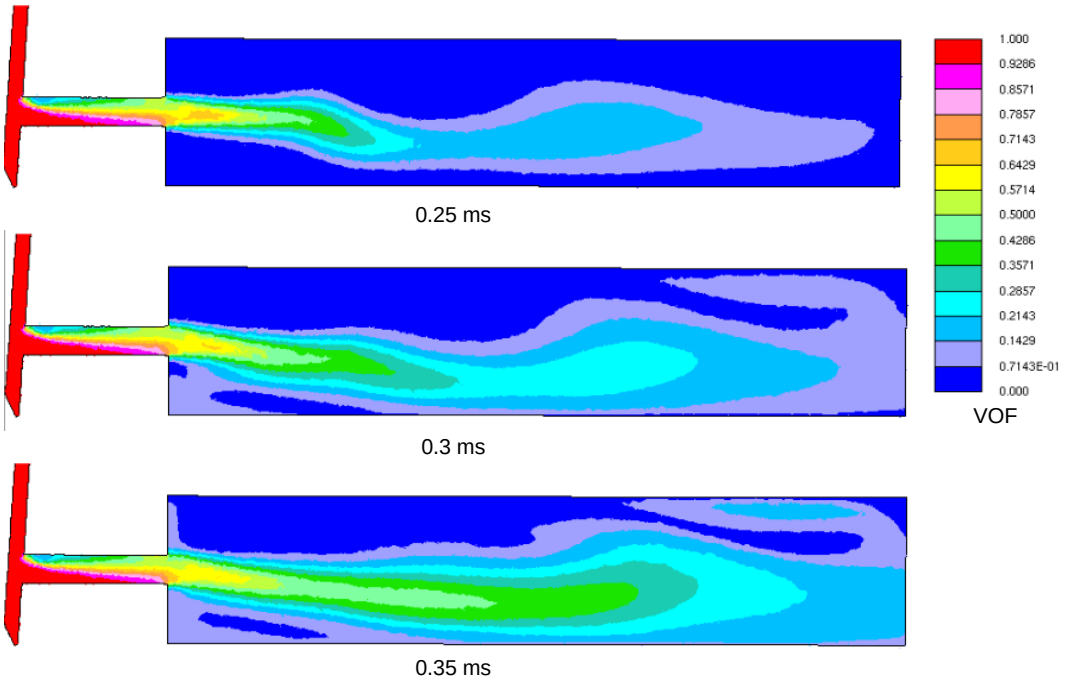

Figure 3. Evolution of the VOF field for Case 1 at 0.2, 0.25 and 0.3 ms ASOI.

The emerging spray jet, for the medium injection pressure case is presented in Figure 4, at time 0.2, 0.25 and 0.25 ASOI. The simulations of the medium pressure case revealed that by increasing the injection pressure for 1124 to 1669, then the required time for the fuel to emerge from the nozzle exit is 0.18 ms. The cavitation area is present at all times after start of injection and the spray jet recirculates at the upper area of the emerging jet at a

downstream distance of seven nozzle diameters. The spray jet core with VOF higher than 0.5, is almost symmetrical and has a length of around five nozzle diameters.

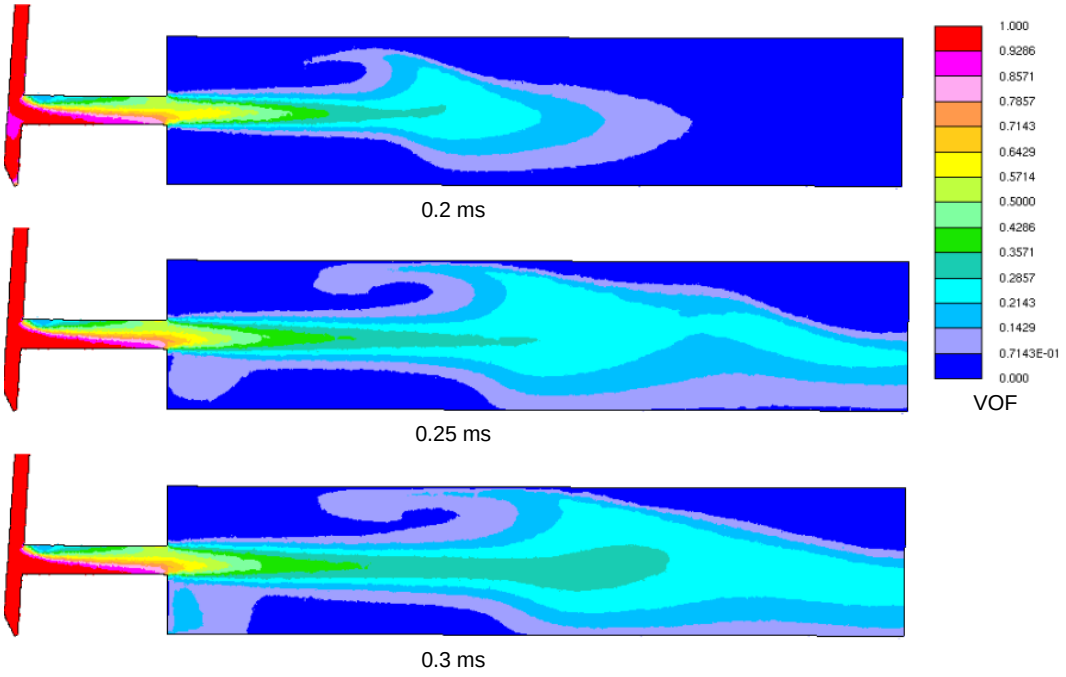

Figure 4. Evolution of the VOF field for Case 2 at 0.2, 0.25 and 0.3 ms ASOI.

The results for Case 3 are included in Figure 5, at 0.15, 0.2 and 0.25 ms ASOI. For the high injection pressure case, the time needed by the fuel to exit the nozzle was 0.14 ms, and this is lower than the time needed for the low and medium injection pressure cases. Figure 4 shows that the vortex structure at the upper area of the spray becomes stronger and that a small amount of fuel accumulates near the wall at the vicinity of the nozzle. Also, it can be observed that the fuel air mixture travels downstream and accumulates towards the front plane of the chamber at 0.25 ms. The VOF and velocity fields for the three are further discussed and compared below.

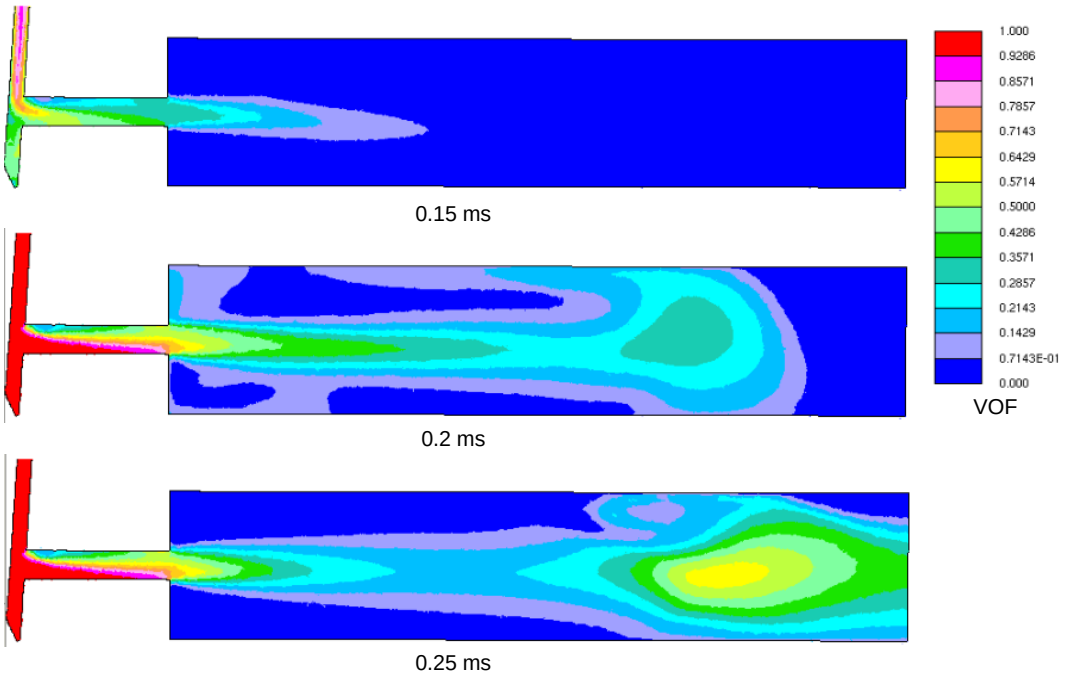

Figure 5. Evolution of the VOF field for Case 3 at 0.15, 0.2 and 0.25 ms ASOI.

EDITORIAL UNIVERSITAT POLITÈCNICA DE VALÈNCIA

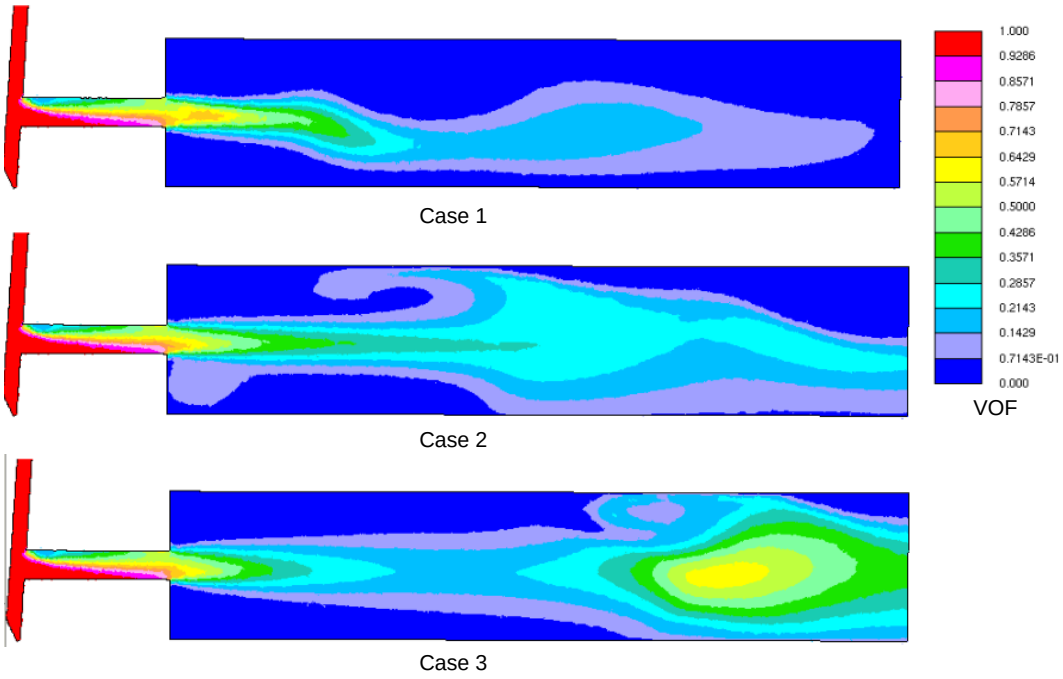

Figure 6. Comparison of the VOF field of Case 1, 2 and 3 at 0.25 ms ASOI.

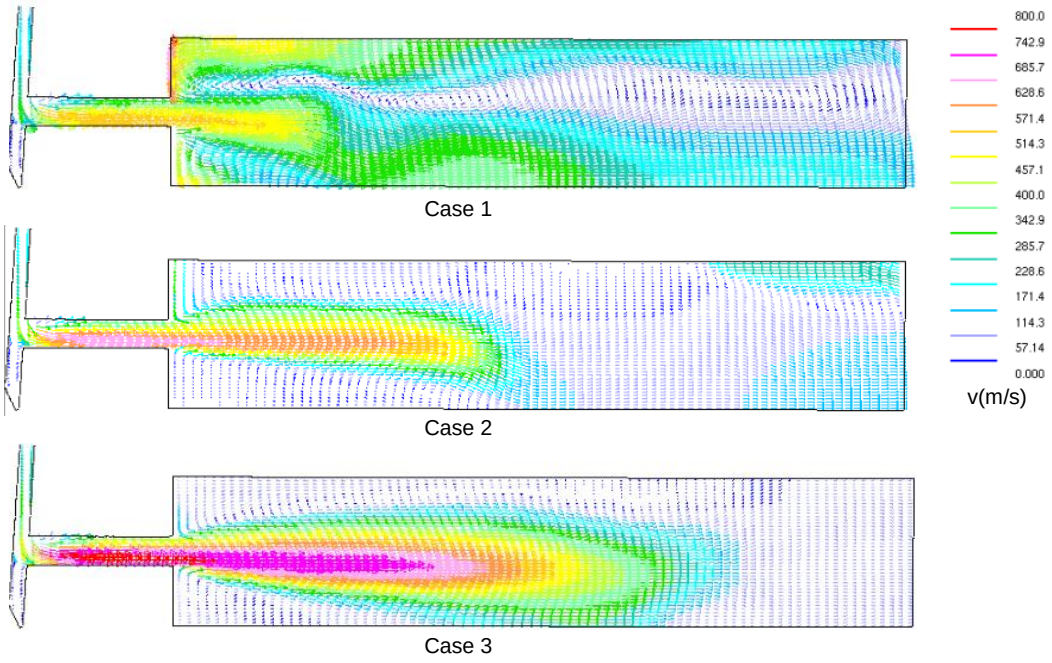

Figure 7. Comparison of the velocity field of Case 1, 2 and 3 at 0.25 ms ASOI.

Figure 6 compares the predicted VOF field at 0.25 ASOI. It can be observed that the spray jet for the low injection pressure case is narrower that the spray of the higher injection pressure cases. This observation reveals that the spray cone angle increases when the injection pressure increases. Regarding the spray jet, it can be seen that the penetration of the spray core with VOF greater than 0.5 increases when the injection pressure increases. However, for the high injection pressure cases there is a core at the vicinity of the nozzle and an accumulated spray jet towards the front plane of the chamber. Figure 7 illustrates the velocity fields for the three cases. The high velocity pattern is wider and longer for the maximum injection pressure case. The latter observation again reveals that the spray cone angle of the high pressure case is larger than the spray angle of the lower pressures. As it can be observed in Figure 7, for all the cases there is a recirculation at the nozzle entry which is the cavitation zone, and the flow has higher velocities at the lower area of the nozzle. By increasing the injection

pressure, then the nozzle velocity increases. The increase of the injection velocity induces a recirculation zone at the upper area of the spray. The recirculation zone becomes stronger with increasing injection velocity and this can be also seen in Figure 6, where the spray recirculation zone occurs for the medium and high injection pressure cases. For the low injection pressure case, the injection velocity is not sufficiently high and the recirculation in upper area affects the spray which slightly bends as observed in Figure 6 and 7.

The estimated breakup length from the simulations is compared against the calculated breakup length from the empirical equation in Figure 4. The time of the start of injection for Case 1, 2, and 3 was adjusted with the values of 0.2, 0.18 and 0.14 ms. This was done for the purpose of comparison, and it is considered as the delay time for the emergence of the liquid jet from the nozzle exit. Figure 8 compares the breakup length data estimated from the simulation against the calculated empirical data for each case. From the simulations, the breakup length was estimated at the distance from nozzle where the VOF value was equal and greater than 0.3. For both the simulation and the experimental data, the breakup length increases with time, as it can be observed in Figure 8. Here, it is noted that the empirical expression does not account for the phenomena of evaporation, while the present simulation was carried out in a chamber with high pressure and temperature conditions and the evaporation was simulated. Thus during the early injection period, for each case, there is slight under prediction of the breakup length and this considered as a very good agreement. However, in Figure 8 it can be seen that for later times the breakup length is substantially underpredicted by the simulation, and this can be explained by the evaporation phenomena which are not considered in the empirical equation.

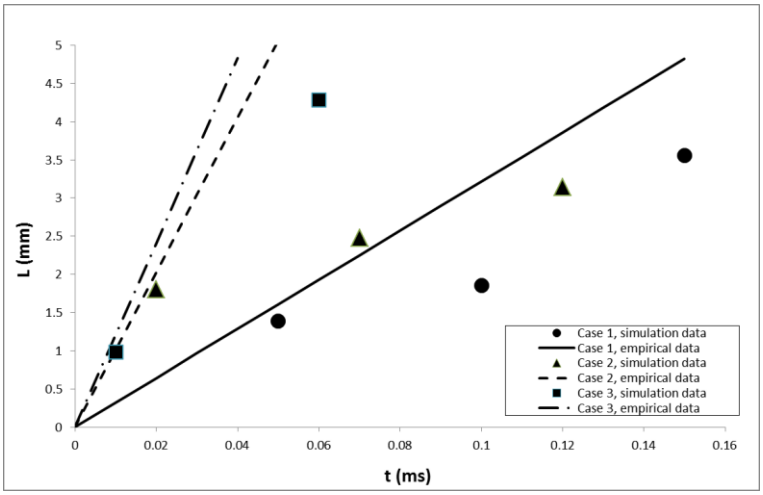

Figure 8. Comparison of the breakup length between simulation and empirical data with elapsed time after the start of injection into the chamber.

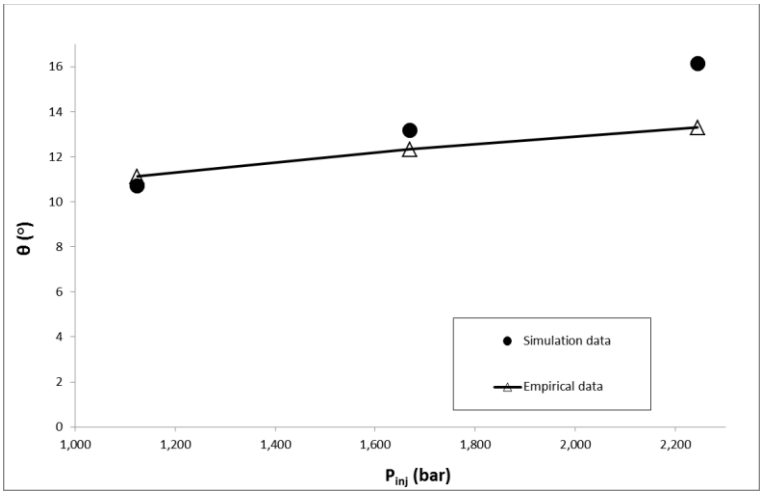

Figure 9. Comparison of the spray jet angle between simulation and empirical data for increasing injection pressure at 0.25 ms ASOI.

The spray jet angle from the simulations was estimated at 0.25 ms ASOI for the three test cases. Tangents from the nozze exit upper and lower edges were drawn to the outer edge of the jet spray at five diameters distance from the nozzle exit, and the average angle for each case was found. The spray cone angle from the simulations for each test case is compared against the empirical data in Figure 9. As it can be seen in Figure 9, there is very good agreement on cone angle for the low injection pressure case, while for the medium and high injection pressure the cone angle is slightly overpredicted. It can be observed that the cone angle increases increases linearly when the injection pressure increases. The differences between the predictions and the empirical data can be explained by the spanwise spreading of the spray jet in the simulation and the interaction with the surrounding gas. However, in order to be able to draw firm conclusions about the overprediction of the cone angle at higher injection pressures, it will be required to carry out further simulation investigation and compare with experimental data. Furthermore, it will be required to assess available empirical data and the conditions under which the empirical expressions can be applied, since in the present work high injection pressures and evaporating conditions were simulated. In the following section, the main conclusions from the present work are described and recommendations for future work are provided.

Conclusions and recommendations

From the three test cases of increasing injection pressure into high pressure and temperature chamber conditions, it was found that cavitation takes place and affects the fuel and air interaction at the upper area of the spray jet. The predicted jet breakup length increases with elapsed time. When the injection pressure increases, then both the breakup length and the downstream penetration of the spray jet increase. The spray cone angle estimated at the vicinity of nozzle exit increases with increasing injection pressure. When the injection pressure doubled, then the cone angle increased by around 50%. Comparisons with empirical data revealed that there is very good agreement on the breakup length size during the early stages of injection, for all the test cases. However, when time elapses from the start of injection then the predicted breakup length is underpredicted because of the evaporation phenomena, which are not accounted in the empirical expression.

In future work a bigger constant volume chamber should be used in order to examine the downstream behaviour of the atomized jet and the resulting downstream spray cone angle. It is recommended to use the predicted values of breakup length and spray cone angle from the present simulations in combination with the Eulerian-Lagrangian framework for simulation of direct injection diesel engine sprays, which should be validated against experimental data in order to reach robust conclusions.

Acknowledgements

The provision of computer facilities by Frederick University is acknowledged.

References

[1] Andriotis, A, Gavaises, M. and Arcoumanis, C., 2008, J. Fluid Mech., 60, pp. 195-215.
[2] Arai, M., Sep. 2.-6. 2012, 12th Triennial International Conference on Liquid Atomization and Spray Systems.
[3] Computational Dynamics adapco Ltd., 2015, STAR-CD Methodology, Version 4.22. London, England.
[4] Dassault Systèmes SolidWorks Corporation, http://www.solidworks.com.
[5] de Villiers, E., Gosman, A. D. and Weller, H. G, 2004, SAE Technical Paper Series 2004-01-0100.
[6] Giannadakis, E., Gavaises, M. and Arcoumanis, C., 2008, J. Fluid Mech., 616, pp. 153-193.
[7] Heywood, J. B. 1987, "*Internal Combustion Engine Fundamentals*"
[8] Jameel, A., Bowen, P., and Yokoi, K., 8.-10. Sep., 2014, *26th* European Conference on Liquid Atomization and Spray Systems.
[9] Margot, X., Hoyas, S., Fajardo, P. and Patouna, S., 2010, Mathematical and Computer Modelling, 52, pp. 1143-1150.
[10] Oda, T., Ohnishi, K., Sumi, T. and Ohsawa, K., Sep. 2.-6. 2012, 12th Triennial International Conference on Liquid Atomization and Spray Systems.
[11] Payri, F., Payri, R., Salvador, F. J. and Martinez-Lopez, J., 2012, Computers & Fluids, 58, pp.88-101.
[12] Payri, F., Salvador, F. J., Marti-Aldaravi, M. and Martinez-Lopez, J., 2012, Energy Conversion and Management, 54, pp.90-99.
[13] Salvador, F. J., Martinez-Lopez, J., Romero, J. V. and Rosello, M. D., 2013, Mathematical and Computer Modelling, 57, pp. 1656-1662.
[14] Sou, A., Pratama, R. H., Tomisaka, T. and Kibayashi, Y., 2.-6. 2012, 12th Triennial International Conference on Liquid Atomization and Spray Systems.
[15] Tamaki, N., Nishikawa, K. and Fukamichi, S., 1.-4. Sep.2013, *25th* European Conference on Liquid Atomization and Spray Systems.
[16] Varde, K. S., 1985, *The Canadian Journal of Chemical engineering* 63
[17] Yakhot, V., and Orszag, S.A. 1986, J. Scientific Computing, 1, pp. 1–51.